Theory of magnetic-field-induced critical end point in $BiMn_2O_5$

Gun Sang Jeon,[1] Jin-Hong Park,[2] Jae Wook Kim,[3] Kee Hoon Kim,[3] and Jung Hoon Han[2,*]
[1]*Department of Physics and Astronomy, Seoul National University, Seoul 151-747, Korea*
[2]*Department of Physics, BK21 Physics Research Division, Sungkyunkwan University, Suwon 440-746, Korea*
[3]*Department of Physics and Astronomy, CSCMR and FRPD, Seoul National University, Seoul 151-747, Korea*
(Received 19 October 2008; revised manuscript received 21 February 2009; published 31 March 2009)

A recent experiment on the multiferroic $BiMn_2O_5$ compound under a strong applied magnetic field revealed a rich phase diagram driven by the coupling of magnetic and charge (dipolar) degrees of freedom. Based on the exchange-striction mechanism, we propose here a theoretical model with the intent to capture the interplay of the spin and dipolar moments in the presence of a magnetic field in $BiMn_2O_5$. Experimentally observed behavior of the dielectric constants, magnetic susceptibility, and the polarization is, for the most part, reproduced by our model. The critical behavior observed near the polarization reversal ($P=0$) point in the phase diagram is interpreted as arising from the proximity to the critical end point.

DOI: 10.1103/PhysRevB.79.104437 PACS number(s): 77.80.−e, 75.30.Fv, 75.47.Lx

I. INTRODUCTION

Beginning with the pioneering work of Hur *et al.*,[1] a series of experiments has uncovered remarkable cross correlations of the magnetic and electric dipole (i.e., polarization) behavior in a class of compounds RMn_2O_5 (R=Tb,Ho,Dy).[2–4] The coupled behavior of the magnetic and polarization degrees of freedom is due in large part to a significant exchange striction in these materials, and to the presence of geometric frustration in the magnetic exchange network. The idea of exchange striction as the driving force of multiferroic behavior in the RMn_2O_5 compound was first proposed in Refs. 3 and 5.

A more recent theoretical advance in regard to the exchange-striction coupling in RMn_2O_5 includes an effective theory formulation[6] and a group-theoretical analysis.[7] A review by Sushkov *et al.*[8] discusses an equation-of-motion method treating the coupled dynamics of spins and the dipole moments, which would give rise to the electromagnons observed in RMn_2O_5 compounds. A key ingredient in the order-parameter-based theories of RMn_2O_5 (Refs. 5–7) is the presence of multiple magnetic order parameters and the interaction between them through coupling to the atomic displacement in describing the observed ferroelectricity.

Our approach here differs from existing models in that we aim to construct an explicit microscopic model for RMn_2O_5. The same exchange-striction idea underlies both our model and the models proposed in Refs. 5–7. In particular, we try in this paper to understand the phase diagram obtained in a recent high magnetic (H) field study on one member of the RMn_2O_5 family, $BiMn_2O_5$ (BMO), which revealed a high-field phase with critical behaviors of the polarization and the magnetization at the point where P (bulk polarization) is tuned through zero.[9]

The experimental findings for BMO under high magnetic field, described in detail in Ref. 9, is the following. In the low-temperature ferroelectric phase of BMO, application of the magnetic field H along the crystallographic a axis in excess of 20 T resulted in a sharp increase in the b-axis dielectric constant, as well as in the slope of a-axis uniform magnetization dM/dH, as the field strength swept through the critical value H_c. The temperature (T)-dependent trace $H_c(T)$ agreed well with the position of $P=0$ separating the low-field $P>0$ from the high-field $P<0$ region,[10] assuming that the $H=0$ state had the $P>0$ polarization to begin with. Down to the lowest temperature measured at 0.66 K, the $P>0$ to $P<0$ crossover appeared to be smooth with no sign of a first-order discontinuity. Furthermore, the behavior of P at 0.66 K near $H=H_c$ was shown to agree well with the power-law $|P|\sim|H-H_c|^{1/3}$, while that of the b-axis dielectric constant was reproduced with $\varepsilon_b(H)-\varepsilon_b(H=0)\sim|H-H_c|^{-2/3}$. A Ginzburg-Landau scheme was employed to explain the observed power-law behavior.[9]

As is obvious from the symmetry consideration, a second-order phase transition at $P=0$ is ruled out because both sides of $P=0$ are already symmetry-broken states. Only a first-order discontinuity or a crossover is left as a possibility. It was then conjectured[9] that a critical end point with an extremely low critical temperature T^* must exist in this material. The observed critical behavior in both P and ε_b at low temperature then follows naturally from the proximity to the putative critical end point, it was claimed.[9]

Given the novelty of the claim and excitement over the possible field-induced critical phenomena in a multiferroic compound, it is desirable to develop a microscopic model that can capture the essential aspect of the observed dielectric and magnetic behavior of BMO under a high magnetic field. Other existing models[5–8] do not describe the impact of high magnetic field on the phase diagram, although an extension to the high-field case may well be possible in other theories, too. It is also our belief that the coupled dynamics of dipolar and magnetic moments in BMO under the nonperturbative regime of strong magnetic field may be better captured in a straightforward microscopic model such as adopted here.

We organize the rest of the paper as follows. In Sec. II, the complex structure of magnetic Mn networks for BMO is reduced to a simple, manageable spin model coupled to lattice displacements. The model naturally embodies the ideas of spin-lattice coupling already proposed for other compounds such as YMn_2O_5.[3] The relation of the frustration in the magnetic exchange network to the local displacement of Mn ions is made transparent. Then in Sec. III a thorough

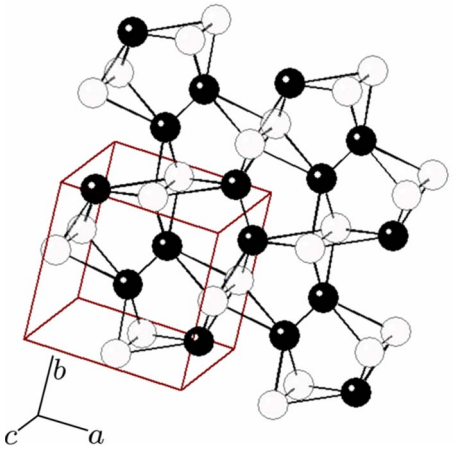

FIG. 1. (Color online) Network of Mn atoms in $BiMn_2O_5$. Filled and empty atoms are $Mn^{3+}(S=2)$ and $Mn^{4+}(S=3/2)$, respectively. A unit cell containing eight Mn atoms is shown as a cube with its axes labeled *a*, *b*, and *c*. Four unit cells are shown in the figure. Bars connecting the atoms have nonzero exchange energies. Exchange interaction between the two Mn^{4+} atoms will be ignored; making the unit cell with six independent spins.

classical Monte Carlo simulation of our model is carried out, both justifying the continuous spin-flop model introduced in Ref. 9 and revealing the power-law behaviors of susceptibilities as in the experiment. The observed exponents agree fairly well with the experimentally measured values even though no quantum-mechanical consideration is given in the present model. The phase diagram for our model is indeed consistent with the presence of a critical end point. We close with a summary and outlook in Sec. IV.

II. MODEL

The pronounced feature of the magnetic structure of BMO is the geometrically frustrated nature of the magnetic interaction pathways. The Mn atoms in BMO occur in two varieties: Mn^{3+} (whose spin is $S=2$ and is surrounded by an oxygen tetrahedron) and Mn^{4+} (spin $S=3/2$, surrounded by an oxygen octahedron). The large spins of both Mn atoms allow us to treat them as classical to the first approximation.

The real-space locations of Mn atoms and their exchange network are presented in Fig. 1. There are eight Mn atoms in a unit cell with four Mn^{3+} and four Mn^{4+} ions each. Three antiferromagnetic exchange interactions have been identified in the literature as dominating the magnetic structure.[2] The two adjacent Mn^{3+} ions (filled circles in Fig. 1) form the strongest exchange bond with J_5. The exchange interaction involving one Mn^{3+} and one Mn^{4+} lying adjacent to it along the *a* axis is the next strongest with J_4. Magnetic exchange of Mn^{3+} with Mn^{4+} lying along the *b* axis is given by J_3, which is the weakest. All three *J*'s are antiferromagnetic. As seen in Fig. 1, a given Mn^{3+} spin is exchange coupled to another Mn^{3+} spin on one side (J_5), and a pair of Mn^{4+} spins on the other (J_4). The two Mn^{4+} spins interact only weakly, and we will ignore this weak exchange of Mn^{4+} spins for the sake of simplicity. As a result, the two Mn^{4+} spins behave identically and there are only six independent spin degrees of freedom

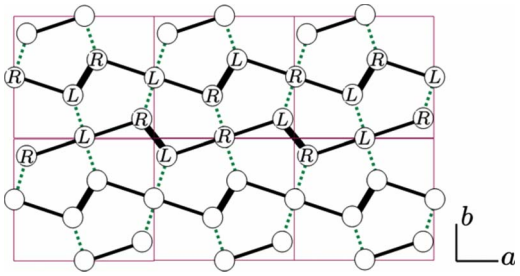

FIG. 2. (Color online) Projection of the Mn network onto the *ab* plane with six atoms per unit cell. Thick and thin full lines represent J_5 and J_4 bonds, while the green dotted lines are J_3 bonds. A sample spin configuration with R (right) and L (left) pointing spins are displayed. The J_3 bonds alternate between being fully satisfied and fully frustrated.

in a unit cell. The approximation to keep only J_3, J_4, and J_5 also makes the system two dimensional.

The six independent spins in a unit cell are coupled to one another in the manner depicted in Fig. 2, where a zigzag chain consisting of alternating $J_5-J_4-J_4-J_5-J_4-J_4-\cdots$ bonds is shown running along the *a* axis. An antiferromagnetic spin configuration is realized for each chain. A weak antiferromagnetic coupling J_3 exists between the chains for a selection of Mn sites connected by dashed lines in Fig. 2. The situation is further simplified in the schematic plot of Fig. 3. Here the geometrically frustrated nature of the Mn exchange is apparent in the form of a closed loop consisting of five Mn spins. Because of this unique connectivity, the interchain interaction cannot be fully satisfied for all J_3 bonds. For a particular realization of antiferromagnetic order on the chains, the interchain antiferromagnetic interaction is alternatively fully satisfied and fully frustrated as one can see in the sample spin configuration of Fig. 2. Translating the spin configuration by one atom for a given chain merely

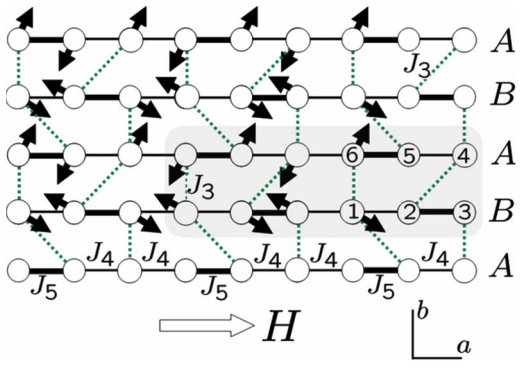

FIG. 3. (Color online) A schematic representation of the Mn network. Thick and thin horizontal links are J_5 and J_4 bonds. The interchain bond J_3 is shown as dotted lines. Two types of alternating chains are labeled as *A* and *B*. A unit cell contains six spins labeled 1 through 6. The magnetic unit cell is twice as large (shaded region). Two kinds of Mn^{3+} pairs, formed by 2–3 and 5–6 atoms, exist in a unit cell. In the experiment of Ref. 9, a magnetic field is applied along the *a* axis as shown and polarization develops along the *b* axis. The spin orientations are antiferromagnetic within a chain, and point in the direction dictated by the local anisotropy, which are different for the two chains.

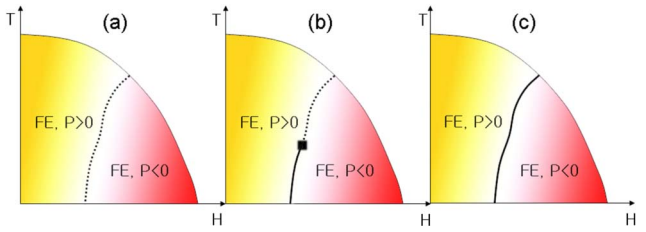

FIG. 4. (Color online) Schematic H-T phase diagram of the model Eq. (2.5) for (a) weak, (b) moderate, and (c) strong spin-lattice coupling χ. The dashed and full lines separating the $P>0$ from $P<0$ ferroelectric (FE) region are crossover and first-order transition lines, respectively, and the dark square in (b) is the critical end point. The scenario (b) is most consistent with known facts about BMO.

shifts the locations of the frustrated bonds by one lattice atom, but fails to relieve the frustration itself. And as a consequence of the frustration, the ground state would possess 2^N degeneracy, N being the number of chains.

In BMO as in other $R\mathrm{Mn_2O_5}$ compounds, the frustration is relieved through the spin-lattice interaction. For a given Mn^{3+} pair (a pair of adjacent Mn^{3+} ions), one Mn^{3+} spin is favorably exchange coupled (antiparallel spins) with the Mn^{4+} spin connected to it, but the other Mn^{3+} spin must be unfavorably coupled (parallel spins) with its neighboring Mn^{4+} spin. Then the Mn^{3+} pair as a whole moves in the direction that strengthens the favorable bond. The relative positions of the Mn^{3+} ions within a pair are assumed to remain rigid during the displacement, while the center of mass of the pair is allowed to move. If all Mn^{3+} pairs are displaced in the same direction, one has a net polarization and a ferroelectric state. There are two types of Mn^{3+} pairs in a unit cell, namely, 2–3 and 5–6 pairs in Fig. 3. Although their movements are not strictly along the b axis in the real compound, it is also known that the a component of the displacements cancels out between the two Mn^{3+} pairs, leaving only the b component to manifest itself in net polarization.[2] In this regard, BMO behaves as a uniaxial ferroelectric.

The unit cell contains six independent spin sites labeled 1 through 6 in Fig. 3. The spin-spin interaction energies within the chain (E_1) and between the chains (E_2) read, respectively,

$$E_1 = J_5 \sum_i (\mathbf{S}_{i2}\cdot\mathbf{S}_{i3} + \mathbf{S}_{i5}\cdot\mathbf{S}_{i6}) + J_4 \sum_i (\mathbf{S}_{i1}\cdot\mathbf{S}_{i2} + \mathbf{S}_{i4}\cdot\mathbf{S}_{i5} + \mathbf{S}_{i3}\cdot\mathbf{S}_{i+\hat{x},1} + \mathbf{S}_{i4}\cdot\mathbf{S}_{i+\hat{x},6}),$$

$$E_2 = J_3 \sum_i (\mathbf{S}_{i1}\cdot\mathbf{S}_{i6} + \mathbf{S}_{i2}\cdot\mathbf{S}_{i4} + \mathbf{S}_{i4}\cdot\mathbf{S}_{i+\hat{y},3} + \mathbf{S}_{i5}\cdot\mathbf{S}_{i+\hat{y},1}), \tag{2.1}$$

repeated over all unit-cell index i. Adjacent cells along the a and b axes are labeled $i\pm\hat{x}$ and $i\pm\hat{y}$, respectively.

The spin-lattice interaction ties the displacement of the Mn^{3+} pairs, or the local dipole moment, with the Mn spin configurations. Each unit cell i contains two Mn^{3+} pairs. The displacement of the 2–3 and 5–6 pairs along the b axis, labeled as d_i and u_i, is subject to the force generated through

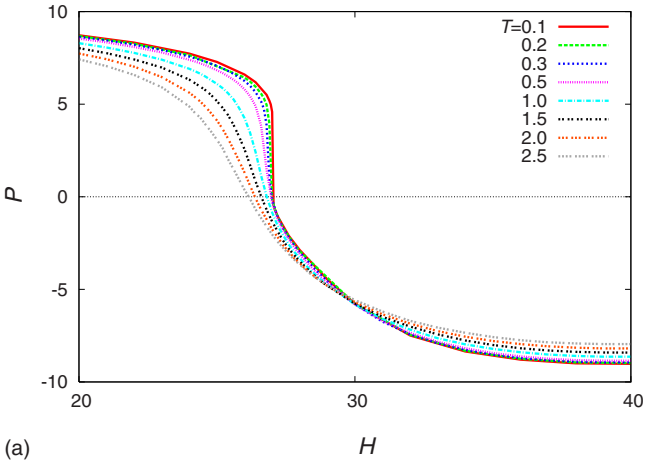

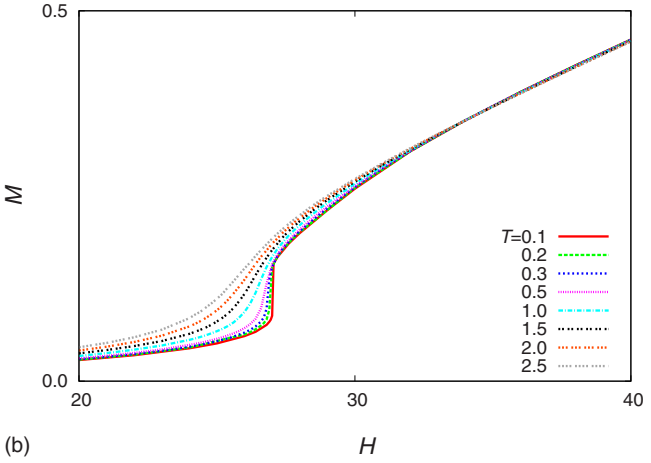

FIG. 5. (Color online) (a) Polarization P and (b) uniform a-axis magnetization M as a function of magnetic field H at various temperatures T. The critical end point occurs between $T=0.1$ and $T=0.2$.

exchange striction. There is also a potential-energy increase associated with the displacements that, up to fourth order, can be written as $\Sigma_i(u_i^2+d_i^2)/2\chi+(\gamma/4)\Sigma_i(u_i^4+d_i^4)$, where χ plays the role of bare dielectric susceptibility and γ is the interaction strength. With the suitable redefinition of χ, u_i, d_i, and γ, one can define the strength of the spin-lattice coupling to be one, and arrive at the spin-lattice interaction energy,

$$E_3 = \frac{1}{2\chi}\sum_i (d_i^2+u_i^2) + \frac{1}{4}\gamma\sum_i (d_i^4+u_i^4) - \sum_i d_i(\mathbf{S}_{i3}\cdot\mathbf{S}_{i-\hat{y},4} - \mathbf{S}_{i2}\cdot\mathbf{S}_{i4}) - \sum_i u_i(\mathbf{S}_{i1}\cdot\mathbf{S}_{i6} - \mathbf{S}_{i5}\cdot\mathbf{S}_{i+\hat{y},1}). \tag{2.2}$$

The last two lines express the exchange-striction effects. Because of the rescaling, we can regard χ as both the bare dielectric susceptibility and the spin-lattice coupling strength.

To the above energies one adds the single-ion anisotropy contribution

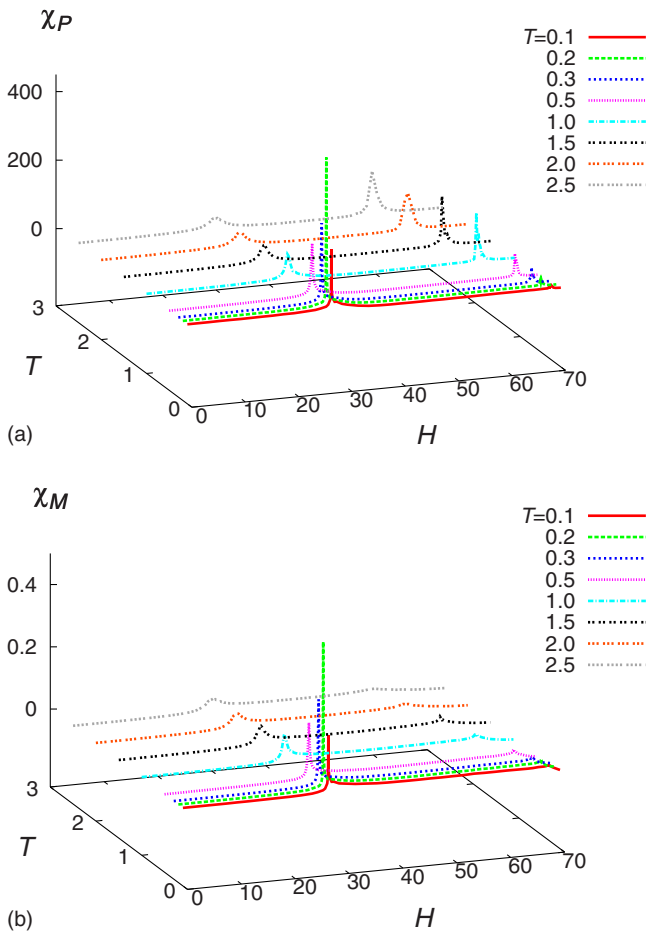

FIG. 6. (Color online) (a) Dielectric susceptibility χ_P and (b) uniform magnetic susceptibility χ_M as functions of magnetic field H and temperature T. The peak occurs near where $P=0$. The peak height rises upon lowering the temperature. The lowest-temperature peak at $T=0.1$ (just below T^*) is smaller than the peak at $T=0.2$ (just above T^*). The second set of peaks at higher magnetic fields are due to the ferro- to paraelectric transition.

$$E_4 = -I\sum_i \sum_{\alpha=1}^{3} (\mathbf{S}_{i\alpha}\cdot\hat{n}_A)^2 - I\sum_i \sum_{\alpha=4}^{6} (\mathbf{S}_{i\alpha}\cdot\hat{n}_B)^2. \quad (2.3)$$

The local anisotropy axes $\hat{n}_A$ and $\hat{n}_B$ are assumed different for the A and B chains. Finally, one adds the Zeeman energy

$$E_5 = -H\sum_i \sum_{\alpha=1}^{6} \mathbf{S}_{i\alpha}\cdot\hat{x}. \quad (2.4)$$

The total energy governing the behavior of spins and displacements in BMO reads

$$E = E_1 + E_2 + E_3 + E_4 + E_5. \quad (2.5)$$

This is the proposed "minimal model" for BMO. In Sec. III we do a classical Monte Carlo simulation of this energy form.

The bulk polarization P is due to the net displacement of the Mn^{3+} pairs,

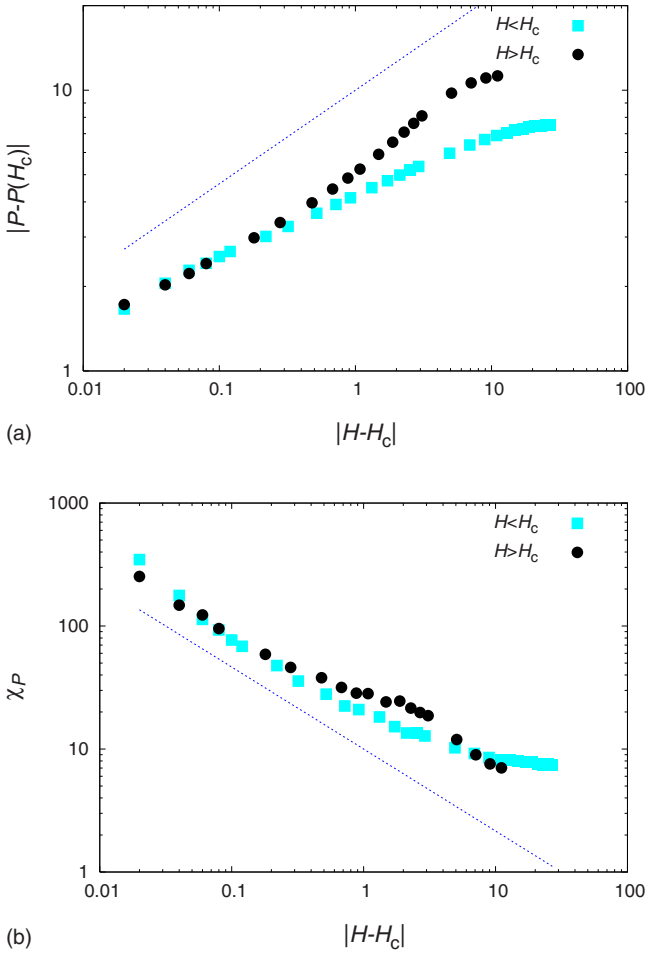

FIG. 7. (Color online) Polarization P and dielectric susceptibility χ_P as functions of magnetic field H at temperature $T=0.2$. The dotted lines represent the power-law behaviors $|P| \propto |H-H_c|^{\alpha'}$ and $\chi_P \propto |H-H_c|^{-\gamma'}$ with the critical field $H_c/J_3=26.92$ and the exponents $\alpha'=1/3$, $\gamma'=2/3$. The errors are at most twice as large as the symbol.

$$P \sim \sum_i (u_i + d_i). \quad (2.6)$$

If we can ignore the quartic interactions in u_i and d_i, the dependence of the local displacements u_i and d_i on the surrounding spin configuration can be worked out exactly, and gives the polarization

$$P \propto \sum_i (\mathbf{S}_{i3}\cdot\mathbf{S}_{i-\hat{y},4} - \mathbf{S}_{i2}\cdot\mathbf{S}_{i4}) + \sum_i (\mathbf{S}_{i1}\cdot\mathbf{S}_{i6} - \mathbf{S}_{i5}\cdot\mathbf{S}_{i+\hat{y},1}). \quad (2.7)$$

Before closing this section it is important to emphasize that the present model is purely classical in its nature. A proper quantum analog will be worked out in the future.

III. MONTE CARLO CALCULATION

An antiferromagnet with the magnetic field applied along the direction of the single-ion anisotropy undergoes a spin-flop process at the critical field $H_c=\sqrt{JI}$, where J and I are

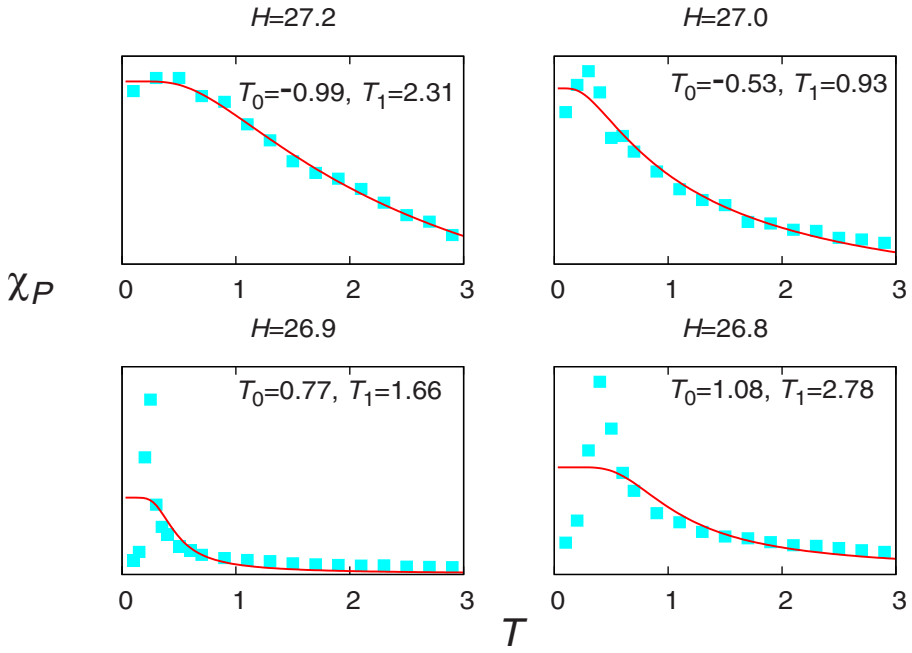

FIG. 8. (Color online) Dielectric susceptibility χ_P (in arbitrary units) as a function of temperature T for various fields. The lines are best fits to Barrett's formula with the two temperature scales T_0 and T_1 as fitting parameters.

the exchange and local anisotropy energies, respectively. If the field direction is not aligned with the anisotropy direction, the spin flop occurs instead in a continuous manner as the spins gradually rotate with H. Such a continuous spin flop can occur in BMO because the local anisotropy directions $\hat{n}_A$ and $\hat{n}_B$ are not strictly parallel to the a axis, the direction of the applied field, but are off by $\pm 8°$.[9] The unique feature of BMO that follows from the different anisotropy directions of the two types of chains (A and B in Fig. 3) is that the spins on the two chains can rotate in the opposite directions with increasing H. If indeed one set of chains has its spins rotate counterclockwise and the other set clockwise, the once antiparallel pair of spins becomes parallel and the parallel spins antiparallel at sufficiently large field strength, and due to a relation such as Eq. (2.7), the polarization direction will get reversed. The salient features of the high-field experiment on BMO (Ref. 9) are summarized here to facilitate the comparison with the Monte Carlo results.

(i) The bulk polarization P along the b axis reverses its direction at a critical field $H=H_c$ applied along the a axis. Near $P=0$ and at the lowest measured temperature $T=0.66$ K, the field dependence of P is consistent with $|P| \sim |H-H_c|^{1/3}$.

(ii) The b-axis dielectric constant ε_b shows a pronounced peak as H is tuned through H_c. The behavior at $T=0.66$ K is consistent with $\varepsilon_b(H)-\varepsilon_b(H=0) \sim |H-H_c|^{-2/3}$.

(iii) The a-axis magnetic susceptibility also shows a peak at $H=H_c$.

(iv) The temperature dependence of $\varepsilon_b(T)$ with the field value fixed at $H \approx H_c$ follows a non-Curie-Weiss form, known as Barrett's formula.[11]

The full lattice model of Eq. (2.5) was treated within the classical Monte Carlo scheme to see if the above-mentioned features of the experiments can be captured within our model. Aided by the experimental input, we consider the planar spins confined in the ab plane, and work with the two-dimensional lattice disregarding the coupling along the c axis. A lattice of $L_x \times L_y$ unit cells, each unit cell consisting of six Mn sites, is considered. We choose the field directed along the a axis as in the experiment,[9] and let H vary from 0 to $+H_{\max}$ for each fixed temperature. The calculation was then repeated for many different temperatures. $H_{\max}$ is chosen in such a way that P evaluated from Eq. (2.6) or (2.7) vanishes before $|H|=H_{\max}$ is reached. Such a field-induced paraelectric transition was continuous, and occurred before the full polarization of spins due to the strong Zeeman field could take place.

A difficulty with the present simulation is the lack of information about the parameter values such as J_3 through J_5 and spin-lattice coupling strength χ. Initially, we worked with several different sets of parameters and later identified the ones which best reproduce the experimental facts. In the course of the general search, we realized that three distinct behaviors (Fig. 4) are possible for the $P>0$ to $P<0$ crossover: (a) with a sufficiently weak χ, the entire $P=0$ line becomes a crossover without a discontinuous jump in P at any temperature. (b) The intermediate range of χ gives the $P=0$ curve that begins as a first-order critical line at low temperature but terminates at a finite temperature, T^*, as a critical end point. The higher-temperature part of the curve becomes a crossover. (c) For a sufficiently strong spin-lattice coupling χ, the entire $P=0$ line is a first-order transition that merges with the second-order paraelectric transition line at high temperature. It is the behavior near the critical end point in scenario (b) that is most relevant for BMO. The Monte Carlo results discussed below are for the parameters that give rise to the scenario (b): $J_4/J_3=J_5/J_3=20$, $\chi/J_3=3$, $I/J_3=9$, and $\gamma=0$. The anisotropy angles θ_A and θ_B, defined by $\hat{n}_A \cdot \hat{x}=\cos\theta_A$, $\hat{n}_B \cdot \hat{x}=\cos\theta_B$, are chosen as $\theta_A=-\theta_B=30°$. The exaggerated anisotropy angle (experimental values are $\pm 8°$)

is a consequence of searching for a parameter set that can produce the critical end-point temperature T^* at a sufficiently low temperature, well below the paraelectric transition.

All calculations were performed on the lattice size $L_x = L_y = 16$ with the periodic boundary conditions in both directions. A standard Metropolis update scheme was used. Due to the complexity of the model, some care was needed in implementing the Monte Carlo program. First, a "typical" configuration at each temperature T for zero field was obtained by means of the simulated annealing method. Then, beginning with the zero-field configuration thus obtained, we increase H to compute physical quantities as functions of T and H. At each temperature and field, at least 2×10^4 Monte Carlo steps per spin and displacement were made, and typically 4×10^3 steps were discarded for equilibration. Near the critical region, more steps of up to 5×10^5 were required for sufficient equilibration and ensemble averages. Throughout the paper we denote energy, temperature, and field in units of J_3.

For a given instantaneous configuration, we compute the magnetization per spin along the field,

$$\mathcal{M} \equiv \frac{1}{6L_xL_y} \sum_i \sum_{\alpha=1}^{6} \mathbf{S}_{i\alpha} \cdot \hat{x}, \tag{3.1}$$

and the polarization per unit cell,

$$\mathcal{P} \equiv \frac{1}{L_xL_y} \frac{1}{J_3} \sum_i (u_i + d_i). \tag{3.2}$$

The average polarization P and magnetization M are then calculated by

$$P = \langle \mathcal{P} \rangle, \quad M = \langle \mathcal{M} \rangle, \tag{3.3}$$

where $\langle \cdots \rangle$ indicates the ensemble average. We can also compute the dielectric (χ_P) and magnetic (χ_M) susceptibilities as

$$\chi_P = \frac{L_xL_y}{T/J_3} (\langle \mathcal{P}^2 \rangle - \langle \mathcal{P} \rangle^2),$$

$$\chi_M = \frac{6L_xL_y}{T/J_3} (\langle \mathcal{M}^2 \rangle - \langle \mathcal{M} \rangle^2). \tag{3.4}$$

Varying the parameters within the scenario (b) of Fig. 4 only gave rise to minor quantitative differences without altering the main results described below. The reduction of $|\theta_A| = |\theta_B|$, for instance, resulted in the overall increase of $|P|$ and enhanced T^*. The introduction of nonzero γ only reduces $|P|$. For these reasons we believe the results presented in the following represent the general features near the critical end point in scenario (b).

In Fig. 5 the polarization P is plotted against H for various temperatures. The behavior at $T=0.1$ showed a jump from $P>0$ to $P<0$ as in a first-order transition. The corresponding a-axis magnetization also undergoes a sudden increase at $H=H_c$. For $T \gtrsim 0.2$, both M and P evolve continuously with a sharp slope at $H=H_c$. The critical-field position H_c itself depends smoothly on the temperature. We note that H_c deduced as the location of $P=0$ in the P vs H plot is numerically slightly different from the positions of the maximum susceptibilities. The same difference also shows up in the experiment,[9] but we do not have a good reason to believe that the small discrepancy has any physical importance.

The susceptibilities χ_P and χ_M from Eq. (3.4) are shown in Fig. 6. Clear peaks in both quantities were found as H crosses H_c, and the heights of both peaks increased upon approaching T^* from above. Both are expected to diverge at the critical end point (H^*, T^*). The peaks grew smaller at $T=0.1$, which lies below T^*. In the experiment both susceptibilities reached maximum peak heights at ~ 5 K and decreased below it. On the other hand, no sign of a first-order transition was found for temperatures below 5 K, and no sign of divergent susceptibilities at or near 5 K. Hence it is incorrect to conclude that ~ 5 K corresponds to T^* in the experiment. Rather, the genuine first-order transition should take place, if at all, below the currently available temperature of 0.66 K. It may be that the decrease in the susceptibility that begins with 5 K is a quantum effect such as the presence of a localized phonon of finite energy.

The polarization P and dielectric susceptibility χ_P at $T=0.2$ (just above T^*) and in the vicinity of $H=H_c$ are further analyzed in Fig. 7. Displayed on a log-log plot, the data are consistent with the power-law exponents $\alpha' = 1/3$ and $\gamma' = 2/3$, the same exponents used to fit the experimentally observed behavior of P and ε_b at $T=0.66$ K. A Ginzburg-Landau argument predicting the same exponents can be found in Ref. 9.

The quantum nature of the displacive phonon mode is reflected in the modification of the Curie-Weiss behavior of the dielectric susceptibility to the one described by Barrett's formula,[11]

$$\chi_P(T) = \frac{M}{(T_1/2)\coth(T_1/2T) - T_0}. \tag{3.5}$$

It was shown that the experimental data for $\varepsilon_b(T)$ fit well to the above formula.[9] In Fig. 8, we attempted to fit several curves of χ_P versus T to the same formula in the vicinity of $H_c(T=0)/J_3 \approx 27.0$, the critical-field value at zero temperature. For $H < H_c(0)$ (lower panel), it is apparent that Barrett's formula does not describe the curves very well. For $H > H_c(0)$ (upper panel), the curves seem to fit reasonably well to the formula, only if we allow for negative values of T_0 although T_0 should play the role of the critical temperature of the ferroelectric transition and remain positive. In contrast, the fit to the experimental data was made with positive T_0 in Ref. 9. Overall, we do not find good agreement of our Monte Carlo data for χ_P to Barrett's formula. A Curie-Weiss fit to the high-temperature side of the data also resulted in negative T_0. To achieve improved agreement between theory and experiment in this regard, we believe it is essential to consider the quantum-mechanical nature of the phonon modes u_i and d_i.

IV. SUMMARY AND OUTLOOK

In this paper, we proposed a minimal model of the magnetic-field-induced critical end point recently observed in $BiMn_2O_5$. A classical energy involving the lattice and spin degrees of freedom and their coupling was written down in

Eq. (2.5) and its properties analyzed with the Monte Carlo method. Our findings are summarized below. The readers will find it useful to compare the following set of results with the summary of the experimental facts given at the beginning of Sec. III.

(i) The bulk polarization P along the b axis did reverse its direction at a critical field $H=H_c$ applied along the a axis. The spins on the A and B chains rotated continuously, and in the opposite directions, under the increasing field. Near $P=0$, and at T slightly above T^*, the field dependence of P was found to be in reasonable agreement with the power-law behavior, $|P| \sim |H-H_c|^{1/3}$.

(ii) The b-axis dielectric susceptibility χ_P shows a pronounced peak as H is tuned through H_c. The behavior at low temperature just above T^* is consistent with $\chi_P \sim |H-H_c|^{-2/3}$.

(iii) The a-axis magnetic susceptibility also shows a peak at $H=H_c$, which reaches a maximum value at T^*.

(iv) The temperature dependence of $\chi_P(T)$ at a fixed field $H \approx H_c$ is generally inconsistent with Barrett's formula.[11] The experimentally observed $\chi_P(T)$ agreed better with Barrett's formula.

In conclusion, the magnetic-field dependence of the polarization, and magnetic and dielectric susceptibilities obtained from our model, proved to capture most of the features of the experiment. The simultaneous rise in the dielectric and magnetic susceptibilities in the continuous spin-flop regime emerges naturally from our model. Other features such as the temperature dependence of the dielectric susceptibility do not agree well with the experimental results. The height of the susceptibility peaks reaches a maximum at T^* in our theory since that is where the expected divergence should take place, but, experimentally, the peak heights reach a maximum at ~ 5 K without showing signs of a first-order transition below that temperature. These discrepancies call for a refinement of the present model that should include, among other things, the quantum nature of the displacive phonon modes expressed as d_i and u_i in Eq. (2.5) and the quantum dynamics of the spins. To what extent the quantum correction will alter the low-temperature behavior of the classical result remains to be explored. It is encouraging, on the other hand, that a simple classical model such as we propose already captures many of the prominent features of the experiment.

Field dependence of the polarization and its reversal in the high-field regime in the $R\mathrm{Mn_2O_5}$ family with $R=\mathrm{Y,Er,Eu,Gd}$, but not Bi, was reported in a series of papers published a few years earlier.[12] The behavior of P under magnetic field in other rare-earth compounds seems more complex than that observed for $\mathrm{BiMn_2O_5}$. The systematic correlation of the polarization reversal with the divergent behavior of the magnetic and dielectric susceptibilities had not been noted previously.

First-principles calculation already exists for the $R\mathrm{Mn_2O_5}$ family with $R=\mathrm{Tb}$,[13] and $R=\mathrm{Dy}$,[14] but none as yet for $R=\mathrm{Bi}$. In view of the high-field phase diagram obtained in $\mathrm{BiMn_2O_5}$ recently, it will be clearly very interesting to have the density-functional calculation carried out in this compound as well. Finally, other members of the $\mathrm{RMn_2O_5}$ family should to a certain extent be subject to the similar microscopic Hamiltonian as the one proposed here for $\mathrm{BiMn_2O_5}$ and might possibly exhibit a high-field behavior similar to those found in Ref. 9. On the other hand, the existence of a critical end point in a given compound depends in a subtle manner on the choice of material parameters which could lead to different types of phase boundaries separating the $P>0$ and the $P<0$ regions as shown in Fig. 4.

A key assumption of our work is that the shift of $\mathrm{Mn^{3+}}$ ions alone can account for the ferroelectric polarization. To be fair, the calculation of Ref. 13 reports the shift of oxygen positions as well as those of $\mathrm{Mn^{3+}}$ in the ferroelectric regime. An x-ray structural analysis by Noda *et al.*[15] revealed the shift of $\mathrm{Mn^{4+}}$ and oxygen positions. However, both these works are for other $R\mathrm{Mn_2O_5}$ compounds, and the extent of connection of their work to $\mathrm{BiMn_2O_5}$ remains to be clarified.

ACKNOWLEDGMENTS

This work was supported in part by the Asia Pacific Center for Theoretical Physics. G.S.J. acknowledges support from the KRF (Grant No. KRF-2007-314-C00075). K.H.K. was supported by the National Research Laboratory (Program No. M10600000238). H.J.H. and K.H.K. acknowledge support from the Korea Research Foundation (Grant No. KRF-2008-314-C00101). The authors thank Sang-Wook Cheong for enlightening discussion.

*hanjh@skku.edu

[1] N. Hur, S. Park, P. A. Sharma, J. S. Ahn, S. Guha, and S.-W. Cheong, Nature (London) **429**, 392 (2004).

[2] L. C. Chapon, G. R. Blake, M. J. Gutmann, S. Park, N. Hur, P. G. Radaelli, and S.-W. Cheong, Phys. Rev. Lett. **93**, 177402 (2004); G. R. Blake, L. C. Chapon, P. G. Radaelli, S. Park, N. Hur, S.-W. Cheong, and J. Rodriguez-Carvajal, Phys. Rev. B **71**, 214402 (2005); C. Vecchini, L. C. Chapon, P. J. Brown, T. Chatterji, S. Park, S.-W. Cheong, and P. G. Radaelli, *ibid.* **77**, 134434 (2008).

[3] L. C. Chapon, P. G. Radaelli, G. R. Blake, S. Park, and S.-W. Cheong, Phys. Rev. Lett. **96**, 097601 (2006).

[4] C. R. dela Cruz, F. Yen, B. Lorenz, M. M. Gospodinov, C. W. Chu, W. Ratcliff, J. W. Lynn, S. Park, and S.-W. Cheong, Phys. Rev. B **73**, 100406(R) (2006).

[5] J. J. Betouras, G. Giovannetti, and J. van den Brink, Phys. Rev. Lett. **98**, 257602 (2007).

[6] Chen Fang and Jiangpoing Hu, EPL **82**, 57005 (2008).

[7] A. B. Harris, Ammon Aharony, and Ora Entin-Wohlman, Phys. Rev. Lett. **100**, 217202 (2008).

[8] A. B. Sushkov, M. Mostovoy, R. Valdés Aguilar, S.-W. Cheong, and H. D. Drew, J. Phys.: Condens. Matter **20**, 434210 (2008).

[9] J. W. Kim, S. Y. Haam, Y. S. Oh, S. Park, S.-W. Cheong, P. A. Sharma, M. Jaime, N. Harrison, J. H. Han, G. S. Jeon, P. Cole-

man, and K. H. Kim, arXiv:0810.1907 (unpublished).

[10] Throughout this paper, we use H_c to refer to both the location of $P=0$ and the field at which the dielectric and magnetic susceptibilities reach a maximum. The two quantities are always in close proximity in the experiment as well as in our simulation.

[11] J. H. Barrett, Phys. Rev. **86**, 118 (1952).

[12] Yu. F. Popov, A. M. Kadomtseva, S. S. Krotov, G. P. Vorob'ev, K. I. Kamilov, M. M. Lukina, and M. M. Tegranchi, Zh. Eksp. Teor. Fiz. **123**, 1090 (2003) [JETP **96**, 961 (2003)]; A. M. Kadomtseva, S. S. Krotov, Yu. F. Popov, G. P. Vorob'ev, and M. M. Lukina, Zh. Eksp. Teor. Fiz. **127**, 343 (2005) [JETP **100**, 305 (2005)]; A. M. Kadomtseva, S. S. Krotov, Yu. F. Popov, and G. P. Vorob'ev, Low Temp. Phys. **32**, 709 (2006).

[13] C. Wang, Guang-Can Guo, and Lixin He, Phys. Rev. Lett. **99**, 177202 (2007); Phys. Rev. B **77**, 134113 (2008).

[14] T. Shen, K. Cao, G.-C. Guo, and L. He, Phys. Rev. B **78**, 134413 (2008).

[15] Y. Noda, H. Kimura, Y. Kamada, Y. Ishikawa, S. Kobayahsi, Y. Wakabayashi, H. Sawa, N. Ikeda, and K. Kohn, J. Korean Phys. Soc. **51**, 828 (2007).